

Li⁺ INTERCALATION CURRENT GENERATION IN AMORPHOUS AND CRYSTALLINE MoS₂: EXPERIMENT AND THEORY

O. Balaban^a, O. Izhyk^a, A. Zaichenko^{a,b}, N. Mitina^b, I. Grygorchak^a, and K. Harhay^b

^a*Department of Applied Physics and Nanomaterials Science, Lviv Polytechnic National University, 79013 Lviv, Ukraine*

^b*Department of Organic Chemistry, Institute of Chemistry, Lviv Polytechnic National University, 79013 Lviv, Ukraine*

Email: oksana.v.balaban@lpnu.ua

Received 1 September 2022; revised 11 February 2023; accepted 11 February 2023

In this work, crystalline and amorphous nano-MoS₂ materials for effective Li⁺-intercalation current generation have been synthesized. The effect of disordering on the structural and electrochemical properties of nano-MoS₂ has been systematically investigated by multiple characterizations: transmission electron microscopy (TEM), X-ray diffraction method and electrochemical measurements. Thermodynamic and kinetic peculiarities of intercalation processes have been studied. Dependences of the change in Gibbs' free energy of the intercalation reaction on the extent of 'guest' lithium loading are analyzed. The distinctive feature of disordered structures is their ability to show colossal lithium 'guest' load, which ensures the specific capacity of the material in cathode processes up to ~2500 mAh·g⁻¹ under the discharge not less than 2.6 V relative to lithium. The diffusion coefficient of lithium cations in the structure of disordered nano-MoS₂ is two orders of magnitude higher than that in the crystalline MoS₂. A quantum-mechanical model of the observed phenomena is suggested.

Keywords: MoS₂ nanoparticles, intercalation, Gibbs' energy, diffusion coefficient, resolvent Green's function

1. Introduction

Nowadays, the rapid development of electric vehicles and alternative energy generation, and the impressive successes of nanoscale electronics and spintronics have especially urgently outlined and determined some profound problems which underlie the fundamental contradictions between the ever-growing needs of the latest circuitry and the capabilities of currently used, traditional technologies of autonomous devices for generating, transforming and storing energy. The existing main electrochemical systems of this technology field had been developed more than a century ago, but the progress made since then can be attributed to the introduction of the technology of so-called electrical double-layer capacitors (supercapacitors) [1–4] and power sources with a lithium anode [5–8]. Power sources are intended to ensure high energy-capacitive indices per unit mass and per unit volume. The operation of such devices is

based on the intercalation mechanism of current generation. However, the values of both the specific capacity and the energy are still far from theoretically possible ones in comparison with the electrochemical equivalent of lithium [9, 10]. It became clear that the success in a significant increase in the energy effectiveness of unit mass and the volume of material cannot be achieved only through an extension of the assortment of new cathode materials [11]; a radical revision of the conceptual approaches is required there [12].

The first steps in this direction were made due to nanotechnology. The transition to the charge-accumulating and energy-generating nanoparticles had enabled us, not very much, but nevertheless to fundamentally improve the effectiveness of intercalation current generation. Thus, the application of nano-dispersed FeS₂ in power sources with a lithium anode increases the specific capacity by almost 20% as compared to the macrocrystallized homologue [13]. Nano-sized α -Fe₂O₃, unlike well-macrostructured

α -Fe₂O₃, γ -Fe₂O₃ and α -Fe₃O₄ exhibited a high reverse specific capacity (200 mAh g⁻¹) and a cyclic ability in the potentials range of 1.5–4.0 V relative to Li⁺/Li reference electrode [14].

The cause of the increase of these parameters for non-metallic nanocrystalline phases can be well accounted for by the concept of ‘electrochemical grafting’ [14, 15]. The essence of this concept is that during the transition to the nanocrystalline state the relative density of states in the energy gap of the material increases. As to its derivation, the density is superficial. This concept caused a rapid growth of works in this direction, which, although approached, however, still did not achieve the goal [16–18]. And only recently [19] we have succeeded in practically achieving such a specific capacity in the cathode process which is close to the gram-equivalent of lithium. It became possible at the expense of maximization of the influence of impurity energy topology by double doping of nano-TiO₂. However, in this case, there were still unresolved problems: increasing the discharge voltage and improving the structure of the discharge curve. This work is devoted to further searching for new approaches to solving these problems.

2. Conceptual approach, materials and methods

2.1. Conceptual approach

Analysis of data from the literature concerning the peculiarities of nanosized particles in intercalation current-generation reactions indicates that it is not only doped but also disordered (amorphous) nanoparticles that are very poorly studied in this perspective. The obtained results [19] unambiguously confirmed the promise of the first approach to increasing the efficiency of intercalation current generation. The second approach has no experimental evidence of its effectiveness, though it is known [20] that it is the amorphization of graphite that causes a triple growth of a specific lithium intercalation capacity; but this takes place only in the anode process.

There is no doubt that it is expedient to use this feature, having switched to the nanoscale, even when the cathode material is concerned. Therefore, it is advisable to choose a semiconductor phase with a layered crystalline structure (for example, a well-known MoS₂ [6–8] for a substantiated comparison)

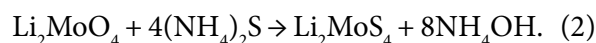
as a cathode material because of the possibility of efficient control over its electronic structure, and hence also the control over the thermodynamics of intercalation current generation in accordance with the Nagelberg–Ozok equation [21]

$$\Delta G(t) = \mu_i(t) - \mu_0 = kT \ln \left| \frac{t_f}{1-t_f} \right| + N\omega t + [E_F(t) - E_F(0)] + L \frac{\partial C}{\partial t} + E_0, \quad (1)$$

where [21] t_f is the fraction of available sites to be filled, t is the number of intercalated atoms of the ‘guest’ component per one structural unit of the ‘host’ material, $\mu_i(t)$ is the chemical potential of the guest component intercalated in the ‘host’ matrix, μ_0 is its chemical potential in the metal anode, k is the Boltzmann’s constant, N is the number of nearby neighbouring places, ω is the interaction energy of the implemented ‘guest’ components, E_F is the Fermi level position, C is the distance between the layers, L is the coefficient determined by the potential function of Lennard-Jones, and E_0 is the guest–host interaction energy. It is clear that the decrease in $\Delta G(t)$ decline can be achieved by purposeful control of the influence of the second and third terms of Eq. (1) due to the controlled change in both the intrinsic and the impurity energy spectra, which will enable us to ‘construct’ the desired form of the discharge curve.

2.2. Synthesis of nanosized molybdenum disulfide

The synthesis of nanosized molybdenum disulfide was carried out as follows. At the first stage, 8.7 g of Li₂MoO₄ was dissolved in 68 ml of 20% (NH₄)₂S. In 30 min (under constant stirring), Li₂MoS₄ dropped in the precipitate according to the reaction:



The obtained Li₂MoS₄ was mixed with 3 ml of hydrazine hydrate N₂H₄·H₂O and with 100 ml of distilled water. After this, the solution was placed in an autoclave with Teflon coating and kept at 180 or 220°C for 24 h. The obtained black precipitate was washed with distilled water and ethanol, and then the precipitate was dried after centrifugation at 40°C temperature.

2.3. Characterization

The size of MoS₂ nanoparticles was studied using the TEM technique by a transmission electron microscope JEM-200A (JEOL, Japan) at 200 kV accelerating voltage. The MoS₂ nanoparticles were dispersed (using an ultrasonic disperser) in distilled water (pH 7.2–7) so that their concentration was 0.1 g per 100 ml. Samples were prepared [22] using the method of spraying the tested solution on a substrate by means of an ultrasonic dispersant UZDN-1A (UkrRosPribor Ltd, Ukraine), which allows for obtaining uniform coating substrates. A thin amorphous carbon film deposited on a copper grid was used as a substrate. The following dispersant options were used: type UZDN-1 possessing 50 W power and 35 kHz frequency.

Crystalline and amorphous structures of MoS₂ nanoparticles were studied using the X-ray diffraction method by an X-ray diffractometer DRON-3 using the known additive method [23]. The size of the particles was calculated by the Scherrer formula $d = k\lambda/(\beta\cos\theta)$, where $k \approx 1$, constant of the instrument, $\lambda = 1.7902\text{Å}$ (CoK α line), the wavelength of the exposure, θ is the angle of diffraction, rad., and β is the physical width of the diffraction maximum, which was calculated by the following formulas: $\beta = (B/2) + (B(B/4 - b/3))^{0.5}$ (for $B \geq 1.5b$) and $\beta = (3b(B - b))/B$ (for $B \leq 1.5b$), where B is the half-width of sample line, rad., and b is the half-width of standard line, rad.

2.4. Electrochemical measurements

For electrochemical studies, electrodes of 0.45 cm² on a nickel mesh were formed. The electrode composition was determined by the proportion of active

material, conductive additive (acetylene black) and binding agent: 85%:10%:5%. The mass of the active material did not exceed 3 mg. The thermodynamic parameters of lithium intercalation were investigated in a three-electrode electrochemical cell with 1M LiBF₄ in γ -butyrolactone, a lithium metal counter-electrode and a chlorine-silver reference electrode.

Electrochemical impedance spectroscopy (EIS) measurements were carried out by using an 'Autolab' (Eco Chemie, the Netherlands) with the frequency analysis module. The amplitude of the signal was 5 mV, and the frequency range was from 10⁻² to 10⁵ Hz. Frequency dependences of complex impedance $Z(f)$ were analyzed using the graph-analytic method in the ZView 2.3 (Scribner Associates) software. The errors of approximation did not exceed 4%.

3. Results and discussion

Figure 1 shows the results of TEM (a) and X-ray spectral analysis (b) of the synthesized MoS₂ nanoparticles. They have the shape of a polyhedron and have dimensions of 20–50 nm. X-ray spectral and X-ray diffraction (Fig. 2(a)) analyses confirm the expected stoichiometric values and hexagonal syngony (space group P6₃/mmc, unit cell parameters are $a = 0.31631 \pm 0.00083$ nm, $b = 1.22097 \pm 0.00781$ nm and $\gamma = 120^\circ$). The decrease in the temperature of the synthesis, even by 40°C, leads to a marked disordering of the structure of nano-MoS₂ (Fig. 2(b)), though with the conservation of the stoichiometry of compound.

As it turned out, the disordering of the structure of molybdenum disulfide nanoparticles radically changes the process of Li⁺-intercalation current generation. Thus, Fig. 3 shows the Gibbs' energy

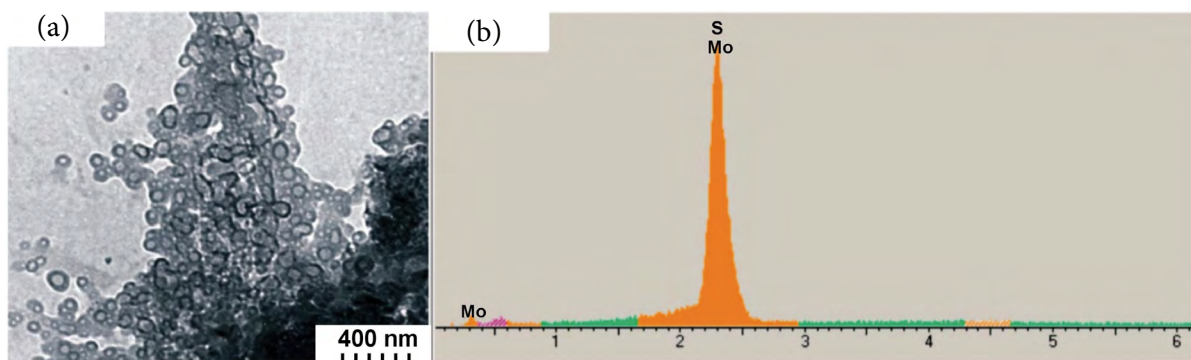


Fig. 1. (a) TEM-image and results of the (b) X-ray spectral analysis of synthesized MoS₂ nanoparticles.

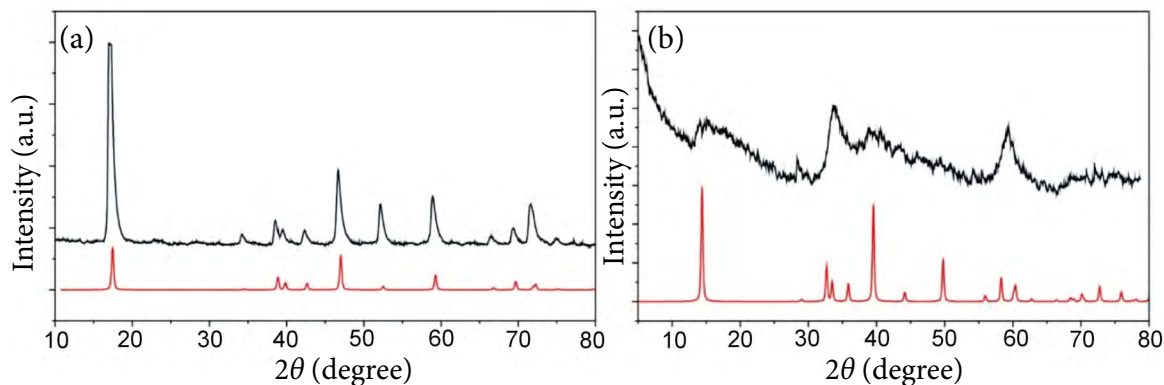


Fig. 2. XRD patterns of the MoS_2 nanoparticles synthesized (upper line) (a) at 220°C and (b) at 180°C and (bottom line) standard XRD patterns for MoS_2 .

change $\Delta G(t)$ of the Li^+ intercalation current-generation reaction of structured nano- MoS_2 versus the specific capacity, which is directly proportional to the degree of ‘guest’ load, and the differential capacity versus the lithium guest load t .

It is evident that in the $0 < t < 0.6$ and $0.6 < t < 2$ concentration intervals of the ‘guest’ load, a series of non-stoichiometric Li_tMoS_2 intercalation compounds were formed. The corresponding chronopotentiograms for each measured value of t are parallel to the t - or capacity axes [24]. With this, the different nature of the dependence of the differential capacity $\partial t/\partial(\Delta G)$ (Fig.3) in the aforesaid intervals indicates that, unlike in the first interval, the mechanism of their formation in the sec-

ond interval is related to the phase transitions of the second kind.

At the same time, the present interval of the constancy of Gibbs’ free energy for the intercalation reaction Li^+ ($2 < t < 2.75$), in which the derivative $\partial t/\partial(\Delta G)$ (Fig. 3) tends to infinity (solid curve), indicates the phase transition of the first kind (the existence of two-phase domain in this interval of the constancy [21]). The emergence of such a phase transition in many cases is due to the strong interaction of ‘guest’ cations with anions of ‘host’, in which a long-range order may occur up to the formation of compounds of a permanent composition. Moreover, when the new phase is in equilibrium with the previous one,

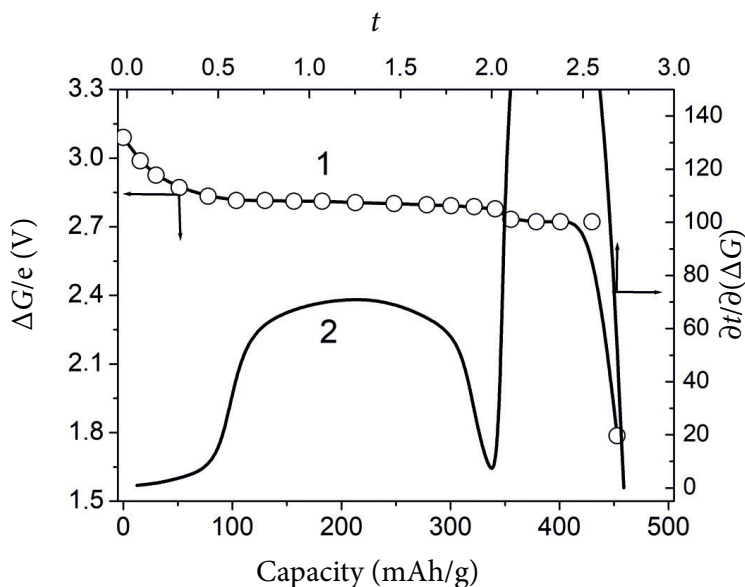


Fig. 3. Gibbs’ energy change (1) versus the specific capacity and differential capacity (2) versus the lithium guest load t during the lithium intercalation process in crystalline Li_tMoS_2 .

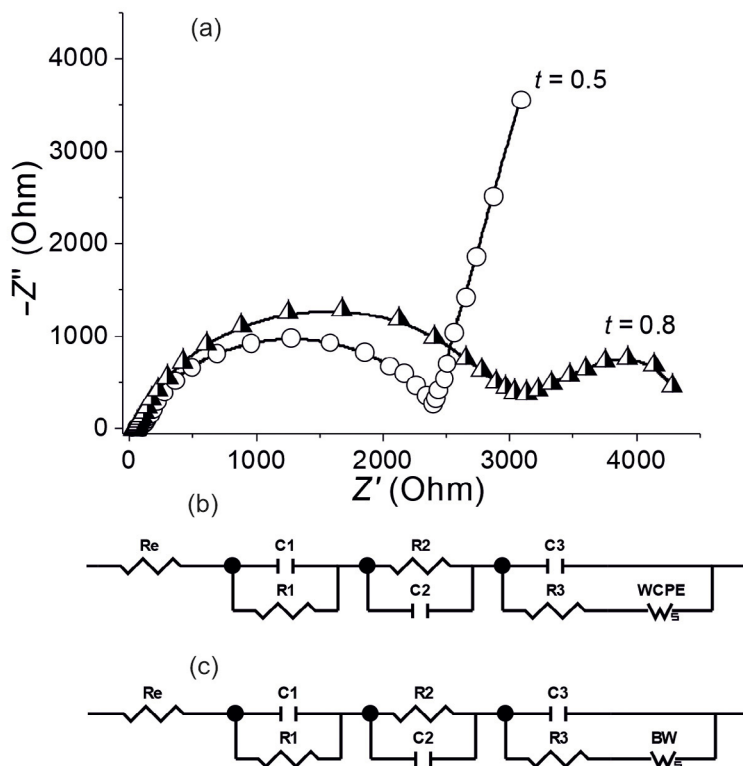


Fig. 4. (a) Nyquist diagrams of the lithium intercalation process in crystalline $\text{Li}_{0.5}\text{MoS}_2$ ($t = 0.5$) and $\text{Li}_{0.8}\text{MoS}_2$ ($t = 0.8$). (b, c) The corresponding electrical circuits.

one can obtain a heterophase system with the corresponding plateau in the $t - \Delta G(t)$ diagram. In the concentration dependence of differential capacity, the neighbourhood of the point of minimum $t \approx 2$ is most often associated with the ordering of the guest subsystem [24].

The kinetics of the Li^+ -intercalation current generation at room temperature in Li_tMoS_2 in the $0 < t < 0.6$ (Fig. 4) interval cannot be described by the classical Randles–Ershler model [25, 26], since the angle of inclination of the low-frequency branches of Nyquist diagrams (Fig. 4(a)) to the axis of the real part of complex impedance differs from 45° . The most likely cause of this is the fact that the diffusion of lithium cations in the molybdenum disulfide nanoparticles is not described by ideal Fick's law. This, in its turn, calls for the application of Warburg (WCDE) (phase deviation $n > 0.5$ index) [25–27] as a structural diffusion element of the distributed impedance in the construction of an impedance model. In the suggested electric circuit (Fig. 4(b)), R_e is the resistance of the electrolyte, $C_3 \parallel (R_3 - W_{CPE})$ is a modified Randles–Ershler link, and parallel links $R_1 \parallel C_1$ and $R_2 \parallel C_2$ represent

the charge transfer through the inter-grain barriers and the passivation film, respectively.

An increase in lithium guest load triggers the second-order phase transitions in the host system in the $0.6 < t < 2$ interval, this also causes changes in the mechanisms of intercalation kinetics. In this case, the type of impedance hodograph unambiguously indicates the impedance of the linear diffusion process, which proceeds in a homogeneous layer of finite thickness. The latter is modelled by the Warburg's kinetic element (BW). Confirmation of the latter can be found from the computer simulation of the electric circuit (Fig. 4(c)), which, in particular, gives the value of the index of phase deviation $n = 0.5$.

Semi-infinite non-ideal diffusion is described by a partial differential equation and is closely related to the change in the thermodynamic characteristics of intercalate phases. It closely links the physical nature of the transformation of this diffusion (to the ideal diffusion), but only in a layer of limited (in relation to the sinusoidal signal) thickness, to the change in the Wagner factor [28], which includes $E(t)$ from Eq. (1). The product

(multiplication) of this factor by ‘physical’ diffusion coefficient (D_0) is a real measurable (chemical) diffusion coefficient $D(t)$. This is well confirmed by the form of $D(t)$ (Fig. 5).

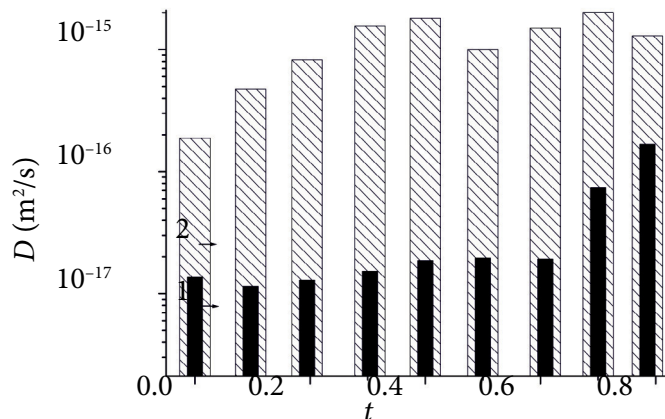


Fig. 5. Histograms of the lithium diffusion coefficient in crystalline (1) and structurally disordered (2) Li_tMoS_2 particles as a function of guest load.

Disordering of the crystalline structure of nanosized MoS_2 leads to a significant increase in the maximum degree of lithium guest load (Fig. 6). For both materials (crystalline and disordered), a series of non-stoichiometric intercalation compounds of Li_tMoS_2 (compare Figs. 3, 6) is formed in the concentration intervals $0 < t < 0.6$ and $0.6 < t < 2$ of the guest load, with further forma-

tion of lithium-arranged structuring Li_2MoS_2 . For $2 < t < 2.75$, instead of the two-phase host-guest states, in the disordered Li_tMoS_2 , one can observe an anomalous shape of $\Delta G(t)$: its increase with an increase in t in $\text{Li}_{2+t}\text{MoS}_2$. The shape of the curve $\Delta G(t)$, according to Eq. (1), at least for the concentration interval $0 < t < 2.75$, is determined mainly by I and III terms. Proceeding from the single-phase state of Li_tMoS_2 for all $0 < t \leq 2$ that is evidenced by differential capacity (Fig. 6), and also taking into account the shape of the curve $\Delta G(t)$ (Fig. 6), its structure is most likely to be associated with a change in the repulsing energy of interaction between adjacent lithium into attracting the energy of interaction. It is the latter that can provide the colossal values of the maximum degree of lithium guest load. Such colossal values are caused by the phase transition of the guest subsystem from the state of lattice gas with fully filled both tetrahedral and free octahedral positions in the van der Waals gap (Li_2MoS_2) to the quasi-liquid $\text{Li}_{2+t}\text{MoS}_2$ (the quantum mechanical model of this phenomenon is illustrated in Ref. [29]). In its turn, this means that the phase transition of the first kind in the interval $2.75 < t < 7.75$ corresponds to the coexistence of intercalating phases of different interaction energy in the quasi-liquid state of the guest subsystem.

Summarizing the received specific discharge capacity of the synthesized materials in comparison with the literature data is presented in Table 1. Here

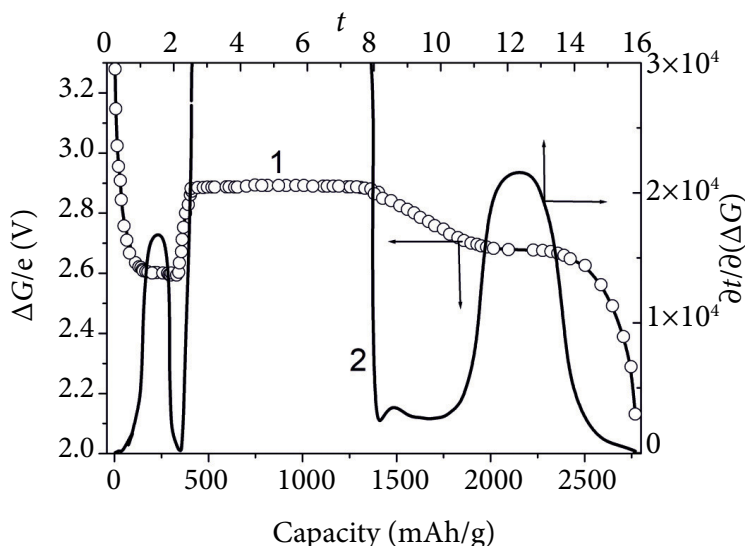


Fig. 6. Gibbs' energy change (1) versus the specific capacity and differential capacity (2) versus the lithium guest load t during the lithium intercalation process in disordered Li_tMoS_2 .

Table 1. Specific capacity of materials.

Material	Structure	Synthesis method	Specific capacity, mAh·g ⁻¹
Crystalline MoS ₂	Crystalline	Hydrothermal	450
Disordered MoS ₂	Amorphous	Hydrothermal	2500
MoS ₂	Flake	–	135 [6]
MoS ₂	Nanosheet	Hydrothermal	1077 [7]
MoS ₂	Hollow nanosphere	Solvothermal	1100 [8]

one can see the energy advantage of amorphous Li_lMoS₂ not only over crystalline Li_lMoS₂ but also over materials from literature. The value of the specific capacity depends on the morphology of the material, as well as on the method of synthesis. The obtained results have been confirmed by the data of thermodynamic research.

4. Theory

The cause of such a peculiar ‘Bose-condensation’ of guest lithium in the amorphous structures of molybdenum disulfide can be accounted for by substantial transformation of the MoS₂ band spectrum during disordering. After all, in the quasiclassical approximation, the latter is considered in the resolvent Green’s function for a two-zone model with the random field U .

In this case, the problem of calculation of the change in the band spectrum, when neglecting the interband interaction, is reduced to finding the Green’s function G , which satisfies the equation:

$$[E - W_l(-i\nabla_x) - U(\mathbf{x})]G_{ll} = -\frac{\hbar}{2\pi}\delta(x-y), \quad (3)$$

$$[E - W_l(-i\nabla_y) - U(\mathbf{y})]G_{ll} = -\frac{\hbar}{2\pi}\delta(x-y). \quad (4)$$

Here, l is the zone index, and $W_l(\mathbf{k})$ is the ‘seed’ dispersion law in the l zone, that is, the dispersion law in the absence of the random field

$$W_l(\mathbf{k}) = -\frac{\hbar^2 k_x^2 + \hbar^2 k_y^2}{2m_l^*} + J_z \cos k_z d_z, \quad (5)$$

where m_l^* , is the effective mass of carriers along the layers, J_z is the integral of interlayer interactions, and d_z is the parameter of lattice that is perpendicular to its layers. The same sense will have the sci-tech terms ‘effective mass’, the boundary of zones, etc.

Having introduced the new variables

$$\mathbf{R} = \mathbf{x} + \mathbf{y}, \quad \mathbf{r} = \mathbf{x} - \mathbf{y}, \quad (6)$$

assuming the smoothness of the random field U (i.e. taking into account only derivatives of the first and the second order) in the expansion of U in \mathbf{r} , we obtain the following expression for the Green’s function:

$$G(E, \mathbf{R}, \mathbf{r}) = \frac{i\hbar}{(2\pi)^4} \int d\mathbf{k} \int_0^\infty ds e^{-\hat{\eta}S} e^{\exp\left[is\left(E\hat{l} - \frac{E_g}{2}\hat{\sigma}_3\right)\right]} \times \\ \times \exp\left\{is\left[\hat{\alpha}\left(\frac{\partial^2}{\partial x^2} + \frac{\partial^2}{\partial y^2} + \frac{\partial^2}{\partial \xi^2} + \frac{\partial^2}{\partial \eta^2}\right) + 2J_z\hat{\sigma}_3\left(\text{ch}\left(d_z\frac{\partial}{\partial z}\right)\text{ch}\left(d_z\frac{\partial}{\partial \zeta}\right) - 1\right) - \hat{I}(U(\mathbf{r}) + r_\alpha r_\beta F_{\alpha\beta})\right]\right\} e^{i\mathbf{k}\mathbf{r}}. \quad (7)$$

Here, \hat{I} , $\hat{\sigma}_3$ are the unit-matrix (further, we shall omit it) and the Pauli matrix, respectively, x , y , z are the coordinates of the vector \mathbf{R} , and ξ , η , ζ are the coordinates of the vector \mathbf{r} .

Using the Feynman scheme of expansion of exponential operators and taking into account the fact that the operators $\text{ch}\left(d_z\frac{\partial}{\partial z}\right)$ are linear combinations of shift operators along the normal to the layers, in the approximation to equilibrium problems, we obtain

$$G(E, \mathbf{R}, \mathbf{r}) = \frac{i\hbar}{(2\pi)^4} \int d\mathbf{k} \int_0^\infty ds e^{-\hat{\eta}S} \exp\left\{is\left[E - \frac{E_g}{2}\hat{\sigma}_3 - u(\mathbf{R}) - \hat{\alpha}(k_x^2 + k_y^2) + 2J_z\hat{\sigma}_3(\cos k_z d_z - 1)\right] + i\mathbf{k}\mathbf{r}\right\}. \quad (8)$$

$$\text{Here } \hat{\alpha} = \frac{\hbar^2}{4} \left[\left(\frac{1}{m_1^*} - \frac{1}{m_2^*} \right) + \left(\frac{1}{m_1^*} - \frac{1}{m_2^*} \right) \hat{\sigma}_3 \right].$$

Conducting averaging over the random field with a Gaussian functionality, one can obtain an expression for the density of states

$$\rho(E) = \frac{1}{\pi\hbar} S_\rho \int d\mathbf{k} \operatorname{Im} \left\{ \frac{i\hbar}{(2\pi)^4} \int_0^\infty ds e^{-\tilde{\eta}s} \exp \left[is \left[E - \frac{E_g}{2} \hat{\sigma}_3 - \hat{\alpha}(k_x^2 + k_y^2) + 2J_z \hat{\sigma}_3 (\cos k_z d_z - 1) \right] - \frac{\psi}{2} s \right] \right\}, \quad (9)$$

where $\psi = \langle u^2 \rangle$ is an average square of random field fluctuations.

Thus, the density of states is an additive magnitude of the densities of the states of individual zones: the conduction $\rho_1(E)$ and the valence $\rho_2(E)$ bands,

$$\rho(E) = \rho_1(E) + \rho_2(E), \quad (10)$$

where $\rho_1(E)$ is determined through the analytical expression

$$\rho_1(E) = \frac{m_1^*}{2\pi\hbar^2 d_z} + \frac{m_1^*}{2\pi^2\hbar^2 d_z} \int_0^\pi \operatorname{erf} \left[\frac{E - E_g/2 + 2J_z(\cos x - 1)}{\sqrt{2\psi}} \right] dx, \quad (11)$$

and $\rho_2(E)$ is the density of states in the valence band. $\rho_2(E)$ has an analytical form that coincides with the analytical form of the density of states in the conduction band after the formal replacement of the effective mass m_1^* by m_2^* and E by $-E$ in the argument of the probabilities integral $\operatorname{erf}(x)$.

Then, besides the substantial transformation of the band spectrum of amorphous Li_2MoS_2 , one should expect an extraordinary effect. Such an effect is accounted for by the acquisition of a mini-zone nature by tails of the density of states. It is caused by the modulating potential of the ordered guest subsystem (at the point $t = 2$) with possible expanding over the Fermi level by one of the bands of localized or delocalized states. Proceeding from Refs. [29, 30], such transformations of the band spectrum can cause a ‘Bose-condensation’ of the lithium guest subsystem in intercalates, its homogeneous or spatially modulated distributions, phase separation and the existence of a ‘reentrant’ transitions (in the case when the ‘Bose-condensate’ phase is an intermediate phase).

The Nyquist diagrams of disordered Li_xMoS_2 are of the same shape as nanocrystallized Li_tMoS_2 (see Fig. 4), but the transition from the semi-infinite non-ideal diffusion to the ideal one in the layer of limited thickness occurs already at $t = 0.3$. At the same time, as should be expected, the diffusion coefficient in disordered nano- Li_tMoS_2 is significantly higher than in the ordered homologue (Fig. 5).

5. Conclusions

1. Disorder the structure of molybdenum disulfide nanoparticles dramatically changes the process of Li^+ -intercalation current generation in MoS_2 – more than five times increases the degree of lithium guest load, and the emergence of the anomalous shape of the Gibbs’ energy change in the range of $2 < t < 2.75$ (its growth with an increase in t) takes place here.

2. The diffusion coefficient of lithium cations in the structure of disordered nanosized molybdenum disulfide is several orders of magnitude higher than that of the nanocrystallized MoS_2 , and the transition from the semi-infinite non-ideal to the ideal diffusion in a layer of limited thickness occurs at significantly lower levels of lithium guest load.

3. It is theoretically proved that for amorphous Li_2MoS_2 we should expect the acquisition of a mini-zone nature by tails of the density of states. It is caused by the modulating potential of the ordered guest subsystem (at the point $t = 2$) with possible expansion over the Fermi level by one of the bands of localized or delocalized states, which, in fact, can provide a ‘Bose-condensation’ of the lithium guest subsystem, its homogeneous or spatially-modulated distributions.

References

- [1] J. Zhao and A.F. Burke, Review on supercapacitors: Technologies and performance evaluation, *J. Energy Chem.* **59**, 276–291 (2021).
- [2] I. Bordun, V. Pohrebennyk, V. Ptashnyk, M. Sadova, and M. Cygnar, in: *Proceedings of the International Multidisciplinary Scientific GeoConference SGEM*, Vol. 2 (Curran Associates, Inc., USA, 2016) pp. 879–886.

- [3] B. Bakhmatyuk and I. Dupliak, Electrochemical performance and the mechanism of process of an electrosorption of iodine by means of the activated carbon material in system of the hybrid supercapacitor, *Nanosistemi Nanomater. Nanotehnologii* **14**(2), 271–283 (2016) [in Ukrainian].
- [4] M.I.A. Abdel Maksoud, R.A. Fahim, A.E. Shalan, M. Abd Elkodous, S.O. Olojede, A.I. Osman, C. Farrell, A.H. Al-Muhtaseb, A.S. Awed, A.H. Ashour, and D.W. Rooney, Advanced materials and technologies for supercapacitors used in energy conversion and storage: a review, *Environ. Chem. Lett.* **19**(1), 375–439 (2021).
- [5] W. Xu, J. Wang, F. Ding, X. Chen, E. Nasybulin, Y. Zhang, and J.-G. Zhang, Lithium metal anodes for rechargeable batteries, *Energy Environ. Sci.* **7**, 513–537 (2014).
- [6] L. Zhang, D. Sun, J. Kang, J. Feng, H.A. Bechtel, L.-W. Wang, E.J. Cairns, and J. Guo, Electrochemical reaction mechanism of the MoS_2 electrode in a lithium-ion cell revealed by *in situ* and *operando* X-ray absorption spectroscopy, *Nano Lett.* **18**(2), 1466–1475 (2018).
- [7] Y. Teng, H. Zhao, Z. Zhang, Z. Li, Q. Xia, Y. Zhang, L. Zhao, X. Du, Z. Du, P. Lv, and K. Świerczek, MoS_2 nanosheets vertically grown on graphene sheets for lithium-ion battery anodes, *ACS Nano* **10**(9), 8526–8535 (2016).
- [8] Y. Wang, L. Yu, and X.W.D. Lou, Synthesis of highly uniform molybdenum-glycerate spheres and their conversion into hierarchical MoS_2 hollow nanospheres for lithium-ion batteries, *Angew. Chem. Int. Ed.* **55**(26), 7423–7426 (2016).
- [9] Y. Zhang, Y. Li, X. Xia, X. Wang, C. Gu, and J. Tu, High-energy cathode materials for Li-ion batteries: A review of recent developments, *Sci. China Technol. Sci.* **58**, 1809–1828 (2015).
- [10] Y.-K. Sun, Direction for development of next-generation lithium-ion batteries, *ACS Energy Lett.* **2**(12), 2694–2695 (2017).
- [11] O.V. Balaban, I.I. Grygorchak, R.M. Peleshchak, O.V. Kuzyk, and O.O. Dan’kiv, The ultrasonic modification of thermodynamic and kinetic regularity of lithium intercalation in talc, *Prog. Nat. Sci. Mater. Int.* **24**(4), 397–404 (2014).
- [12] B.A. Lukiyanets and D.V. Matulka, Peculiarities of electron-electron interaction in quantum-dimensional objects, *J. Nano-Electron. Phys.* **10**(2), 02003-1–6 (2018).
- [13] S.H. Yang, S. Osmialowski, and Q.C. Horn, Nano- FeS_2 for commercial LiOFeS_2 primary batteries, *J. Electrochem. Soc.* **149**, A1499–A1502 (2002).
- [14] M. Quintin, O. Devos, M. Delville, and G. Campet, Study of the lithium insertion–deinsertion mechanism in nanocrystalline $\gamma\text{-Fe}_2\text{O}_3$ electrodes by means of electrochemical impedance spectroscopy, *Electrochim. Acta* **51**(28), 6426–6434 (2006).
- [15] C. Kwon, S. Hwang, A. Poquet, N. Treuil, G. Campet, J. Portier, and J.H. Choy, in: *New Trends in Intercalation Compounds for Energy Storage*, Vol. 61, eds. C. Julien, J.P. Pereira-Ramos, and A. Momchilov (Springer, The Netherlands, 2002) pp. 439–44.
- [16] S. Goriparti, E. Miele, F. Angelisa, E. Fabrizio, R. Zaccaria, and C. Capiglia, Review on recent progress of nanostructured anode materials for Li-ion batteries, *J. Power Sources* **257**, 421–443 (2014).
- [17] F. Wu, N. Li, Y. Su, L. Zhang, L. Bao, J. Wang, L. Chen, Y. Zheng, L. Dai, J. Peng, and S. Chen, Ultrathin spinel membrane-encapsulated layered lithium-rich cathode material for advanced Li-ion batteries, *Nano Lett.* **14**, 3550–3555 (2014).
- [18] S.-T. Myung, F. Maglia, K.-J. Park, C. Yoon, P. Lamp, S.-J. Kim, and Y.-K. Sun, Nickel-rich layered cathode materials for automotive lithium-ion batteries: achievements and perspectives, *ACS Energy Lett.* **2**, 196–223 (2017).
- [19] I. Grygorchak, I. Myronyuk, M. Micov, A. Pidluzhna, and O. Ostapuk, Gigantic capacitoe-energetic parameters of lithium-intercalation current generation reaction in nanodispersed TiO_2 with defective structure, *Acta Phys. Pol. A* **117**, 189–194 (2010).
- [20] K. Yanagida, A. Yanai, Y. Kida, A. Funahashi, T. Nohma, and I. Yonezu, Carbon hybrids graphite-hard carbon and graphite-coke as negative electrode materials for lithium secondary batteries charge/discharge characteristics, *J. Electrochem. Soc.* **149**, A804–A807 (2002).

- [21] A. Nagelberg and W. Worrell, Alkali metal intercalated transition metal disulfides: a thermodynamic model, *J. Sol. State Chem.* **38**, 321–334 (1981).
- [22] G. Schimmel, *Elektronen mikroskopische Methodik* (Springer-Verlag, Berlin-Heidelberg-New York, 1969).
- [23] G. Brindley and G. Brown, *Crystal Structures of Clay Minerals and Their X-ray Identification* (Mineralogical Society, London, 1980).
- [24] J.E.B. Randles, Kinetics of rapid electrode reactions, *Discuss. Faraday Soc.* **1**, 11–19 (1947).
- [25] B. Ershler, Investigation of electrode reactions by the method of charging-curves and with the aid of alternating currents, *Discuss. Faraday Soc.* **1**, 269–277 (1947).
- [26] S. Dhillon and R. Kant, Theory for electrochemical impedance spectroscopy of heterogeneous electrode with distributed capacitance and charge transfer resistance, *J. Chem. Sci.* **129**, 1277–1292 (2017).
- [27] A.H. Thompson, Electrochemical studies of lithium intercalation in titanium and tantalum dichalcogenides, *Physica B+C* **99**, 100–106 (1980).
- [28] A.M. Gusak and N. Storozhuk, Two remarks on Wagner integrated diffusion coefficient, *Metallophys. Adv. Technol.* **41**(5), 583–593 (2019).
- [29] B. Bakhmatyuk, B. Venhryn, I. Grygorchak, M. Micov, and Yu. Kulyk, On the hierarchy of the influences of porous and electronic structures of carbonaceous materials on parameters of molecular storage devices, *Electrochim. Acta* **52**, 6604–6610 (2007).
- [30] I. Stasyuk and V. Krasnov, Phase transitions in Bose-Fermi-Hubbard model in the heavy fermion limit: Hard-core boson approach, *Condens. Matter Phys.* **18**(4), 43702: 1–20 (2015).

ĮTERPTŲ Li^+ JONŲ SROVĖS GENERAVIMAS AMORFINIAME IR KRISTALINIAME MoS_2 : EKSPERIMENTAS IR TEORIJA

O. Balaban ^a, O. Izhyk ^a, A. Zaichenko ^{a,b}, N. Mitina ^b, I. Grygorchak ^a, K. Harhay ^b

^a *Lvivo nacionalinio politechnikos universiteto Taikomosios fizikos ir nanomedžiagų mokslo katedra, Lvivas, Ukraina*

^b *Lvivo nacionalinio politechnikos universiteto Chemijos instituto Organinės chemijos katedra, Lvivas, Ukraina*